# Electronic transitions of iron in almandine-composition glass to 91 GPa

Susannah M. Dorfman[1], Sian E. Dutton[2], Vasily Potapkin[3], Aleksandr I. Chumakov[4], Jean-Pascal Rueff[5,6], Paul Chow[7], Yuming Xiao[7], Robert J. Cava[8], Thomas S. Duffy[9], Catherine A. McCammon[3], and Philippe Gillet[10]

1: Department of Geological Sciences, Michigan State University, East Lansing, MI 48824.
2: Department of Physics, University of Cambridge, Cambridge CB3 0HE, UK.
3: Bayerisches Geoinstitut, University of Bayreuth, 95440 Bayreuth, Germany.
4: European Synchrotron Radiation Facility, BP 220, F-38043 Grenoble, France.
5: Synchrotron SOLEIL, L'Orme des Merisiers, BP 48 Saint-Aubin, F-91192 Gif-sur-Yvette, France.
6: Sorbonne Universités, UPMC Université Paris 06, Laboratoire de Chimie Physique-Matière et Rayonnement, F-75005, Paris, France.
7: HPCAT, Geophysical Laboratory, Carnegie Institution of Washington, Argonne, Illinois 60439, USA.
8: Department of Chemistry, Princeton University, Princeton, NJ 08544, USA.
9: Department of Geosciences, Princeton University, Princeton, NJ 08544, USA.
10: Earth and Planetary Science Laboratory, Ecole polytechnique fédérale de Lausanne, Station 3, CH-1015 Lausanne, Switzerland.

## Abstract

Valence and spin states of Fe were investigated in a glass of almandine ($Fe_3Al_2Si_3O_{12}$) composition to 91 GPa by X-ray emission spectroscopy and energy- and time-domain synchrotron Mössbauer spectroscopy in the diamond anvil cell. Changes in optical properties, total spin moment and Mössbauer parameters all occur predominantly between 1 bar and ~30 GPa. Over this pressure range, the glass changes from translucent brown to opaque and black. The total spin moment of the glass derived from X-ray emission spectroscopy decreases by ~20%. The two Mössbauer spectroscopy approaches reveal consistent changes in sites corresponding to 80-90% $Fe^{2+}$ and 10-20% $Fe^{3+}$. The high-spin $Fe^{2+}$ doublet exhibits a continuous decrease in isomer shift and increase in line width and asymmetry. A high-spin $Fe^{3+}$

doublet with quadrupole splitting of ~1.2 mm/s is replaced by a doublet with quadrupole splitting of ~1.9 mm/s, a value higher than all previous measurements of high-spin $Fe^{3+}$ and consistent with low-spin $Fe^{3+}$. These observations suggest that $Fe^{3+}$ in the glass undergoes a gradual transition from high to low spin state between 1 bar and ~30 GPa. Almandine glass is not expected to undergo any abrupt transitions in electronic state at deep mantle pressures.

Keywords: silicate glass; spin transitions; Mössbauer spectroscopy; nuclear forward scattering; X-ray emission spectroscopy

## 1. Introduction

The high-pressure behavior of Fe-rich silicate liquids is key to the differentiation of the mantle from a primordial magma ocean (Labrosse et al. 2007; Stixrude et al. 2009; Lee et al. 2010) and to understanding observations of possible dense melt-rich regions near the core-mantle boundary (Williams and Garnero 1996). The dynamics of melt in the deep mantle is largely controlled by the behavior of Fe, Earth's densest major elemental component. A density crossover in the deep mantle, with negatively-buoyant Fe-rich silicate melt relative to solid mantle silicates, has been suggested based on the compressibility of melt (Stixrude et al. 2009; Thomas et al. 2012; Muñoz Ramo and Stixrude 2014) and partitioning of Fe into the liquid phase (Nomura et al. 2011; Andrault et al. 2012). However, detailed characterization of mantle melt is challenging due both to experimental difficulty of stable melting at mantle pressures and limited capability to probe liquid structures at extreme conditions. As low-temperature analogues to melts, silicate glasses have been explored in recent high-pressure experiments (e.g. Nomura et al. 2011) and computational studies (e.g. Stixrude and Karki 2005). In both silicate liquids and

glasses a range of coordination environments may evolve continuously with composition and pressure (Stixrude and Karki 2005), but a surprising sharp transition was recently reported at ~70 GPa in Fe-bearing melt and glass and attributed to a spin transition (Nomura et al. 2011).

Spin transitions in crystalline mantle phases and their implications for seismic properties and chemical partitioning have been the focus of much recent study, particularly of ferropericlase (Badro et al. 2003) and silicate perovskite (Badro et al. 2004). In ferropericlase, a spin transition occurs in 6-fold-coordinated $Fe^{2+}$ at pressures between 50 and 90 GPa, depending on Fe content (Speziale et al. 2005; Fei et al. 2007). In silicate perovskite (now known as bridgmanite), the presence of multiple sites and valence states makes characterizing the spin state more complex, but both experiments and density functional theory results indicate that a spin transition occurs in 6-fold-coordinated $Fe^{3+}$ at 15-50 GPa (Catalli et al. 2010; Hsu et al. 2011; Lin et al. 2012). At high temperatures relevant to Earth's mantle, the effects of Boltzmann statistics and kinetics have been predicted (Sturhahn et al. 2005; Tsuchiya et al. 2006; Lin and Tsuchiya 2008) and observed (Lin et al. 2007; Kantor et al. 2009) to broaden each of these spin transitions to occur over a pressure interval extending for ~30-50 GPa.

Liquids and glasses are characterized by continuous structural evolution under compression that may also contribute to the pressure-broadening of spin transitions. At mantle temperatures, the spin transition in liquid $Fe_2SiO_4$ has been predicted to take place over a >200 GPa pressure range (Muñoz Ramo and Stixrude 2014). While this transition might affect the depth of a solid-liquid density crossover in the mantle, it would not be observable as a discontinuity. In contrast, Nomura et al. (2011) reported a sharp change in Fe partitioning in partially-melted $(Mg_{0.89}Fe_{0.11})_2SiO_4$ between 73 and 76 GPa. At similar pressures, between 59

and 77 GPa, they also observed that X-ray emission spectra of $(Mg_{0.95}Fe_{0.05})SiO_3$ glass indicated a complete spin transition. Other studies are not consistent with abrupt spin transitions in liquids and melts. No sharp change in partitioning was observed in chondritic melt at pressures up to 120 GPa (Andrault et al. 2012). Studies of several different Fe-bearing silicate glass compositions—10-50% $FeSiO_3$, $Fe^{3+}/\Sigma Fe$ from 0-78%, with and without Al—showed either no change in spin state (Mao et al. 2014; Prescher et al. 2014) or a gradual, partial change (Gu et al. 2012; Murakami et al. 2014) at high pressures. Gradual increases in cation coordination rather than spin transitions were inferred to be primarily responsible for pressure-induced changes in these glasses (Mao et al. 2014; Prescher et al. 2014).

Studies of Fe spin state at extreme pressures rely on two complementary synchrotron techniques: X-ray emission spectroscopy and Mössbauer spectroscopy. X-ray emission spectroscopy (XES) measures energies of electron exchange between 3*p* and 3*d* orbitals, which depend on bonding, coordination, valence and spin states (Peng et al. 1994; Rueff et al. 1999; Mattila et al. 2007). This technique was the first used to identify pressure-induced spin transitions in major lower mantle phases (Badro et al. 2003, 2004). However, XES only provides a constraint on the total spin moment of the bulk material, not of individual states or sites. Mössbauer spectroscopy provides a complementary constraint on coordination, site occupancy, valence, and spin states of Fe via the energies of recoil-free nuclear resonance in solid materials. The technique can be applied to glasses but not silicate liquids; for insights on melt structures, a wide variety of silicate glass compositions have been examined at ambient pressure by Mössbauer spectroscopy (MS) with a conventional radioactive source (e.g. Mao et al. 1973; Virgo and Mysen 1985; Jayasuriya et al. 2004; Dunlap and McGraw 2007; Rossano et al. 2007;

Cottrell and Kelley 2011). $^{57}$Fe nuclei of each site, species and spin state resonate at energies with isomer shift (IS), quadrupole splitting (QS) and hyperfine splitting that reflect the local electric and magnetic fields. The relative intensities of each site indicate the abundance of $Fe^{2+}$ and $Fe^{3+}$ in each spin state and coordination environment. For Mössbauer spectroscopy of materials at high pressures, synchrotron radiation can provide a more brilliant, highly-focused source. Energy-domain synchrotron Mössbauer spectroscopy (E-SMS) is identical to MS with the exception of a more brilliant source obtained by monochromatizing a synchrotron beam to ~neV linewidth (Smirnov et al. 1997; Mitsui et al. 2009; Potapkin et al. 2012). Mössbauer parameters IS and QS can also be derived from nuclear forward scattering (also known as time-domain synchrotron Mössbauer spectroscopy, T-SMS), in which nuclear resonance is observed in ~few hundred nanosecond time windows between pulses of synchrotron radiation (Jackson et al. 2005; Sturhahn et al. 2005). The combination of XES, E-SMS and T-SMS techniques offers the best approach for separation of competing effects and thus understanding complex Fe-bearing materials such as silicates at lower mantle conditions.

Fe,Al-bearing silicate glass compositions examined in previous studies are rich in ferric iron; glass of almandine garnet composition provides a useful contrast as it is rich in both aluminum and ferrous iron. Almandine is also of particular interest among silicate minerals for its unusual electronic structure, with high quadrupole splitting at ambient conditions and at high pressures (Dyar et al. 2006; Mao et al. 2013). At ~80 GPa and 2500 K, almandine end-member $Fe_3Al_2Si_3O_{12}$ has been observed to transform to a single-phase orthorhombic perovskite consistent with stoichiometry $(Fe_{0.75}Al_{0.25})(Al_{0.25}Si_{0.75})O_3$ (Dorfman et al. 2012). Structural

refinement of X-ray diffraction data for this phase shows that nearly all Fe resides in the larger A-site and there are no discontinuities in its equation of state up to 150 GPa.

In this work, we apply multiple techniques to characterize the pressure-dependence of valence and spin states in almandine glass at pressures up to 91 GPa. Total spin moment is determined by XES. Valence, spin, and coordination states are constrained by E-SMS and T-SMS.

## 2. Material and methods

$^{57}$Fe-enriched almandine glass was prepared from a stoichiometric mixture of $^{57}Fe_2O_3$ (Cambridge Isotope Laboratories, Inc., $^{57}$Fe 94.3%), $Al_2O_3$ (Alfa Aesar 99.9%) and $SiO_2$ (Johnson Matthey, 99.995%) after the method described by Geiger et al. (1987). Approximately 300 mg of reagents were placed in a covered graphite crucible and heated from 1000°C to 1200°C at a rate of 4°C/min. The sample was held at 1200°C for 6 minutes before being quenched in air. To ensure a homogeneous product the resultant material was subsequently arc melted under an argon atmosphere. The composition and homogeneity of the glass were confirmed by microprobe analysis (Supplementary Table 1). The normalized formula, $Fe_{2.69}Al_{2.14}Si_{2.93}O_{12}$, is slightly depleted in Fe and enriched in Al relative to pure almandine.

The valence state of Fe in the starting material was determined by Mössbauer spectroscopy. MS was performed over ~1 day with a $^{57}$Co radioactive source at the Advanced Photon Source (APS) sector 3 offline Mössbauer laboratory. The spectrum was fit to a two-site model (Figure 1, Table 1) using MossA software (Prescher et al. 2012). The dominant site, 82(3) percent of the iron, has QS of 2.08(3) mm/s and IS relative to an iron standard of 0.982(14)

mm/s. These parameters are typical of $Fe^{2+}$ in silicates (Dyar et al. 2006) and glasses (Dyar 1985; Virgo and Mysen 1985; Burkhard 2000; Jayasuriya et al. 2004; Mysen 2006; Rossano et al. 2007; Gu et al. 2012; Mao et al. 2014; Murakami et al. 2014; Prescher et al. 2014). The QS of $Fe^{2+}$ in almandine glass is considerably lower than the 3.53 mm/s observed in crystalline almandine (Woodland and Ross 1994; Dyar et al. 2006). A significant minority site was observed with QS=1.23(11) mm/s and IS=0.39(5) mm/s, consistent with $Fe^{3+}$ in silicate glasses but with higher QS than $Fe^{3+}$ in silicate garnets. This analysis yields $Fe^{3+}/\Sigma Fe$ of 18(3)%.

High-pressure experiments were performed using symmetric diamond anvil cells (DAC). Glass samples were loaded with a ~8 μm ruby ball in NaCl, cryogenically-cooled Ar or pressurized Ne (Rivers et al. 2008) (Figure 2). A 50 to 80-μm diameter hole was drilled through a Re or Be gasket to serve as a sample chamber. Diamond anvils with 150, 200 and 300-μm culet size were used in separate experiments to reach maximum pressures of 91, 86, and 66 GPa, respectively. Pressure was calibrated by ruby fluorescence (Mao et al. 1986) or Raman spectroscopy of the tip of the diamond anvil (Akahama and Kawamura 2006).

XES was performed at pressures up to 66 GPa at beamline GALAXIES of Synchrotron SOLEIL (Rueff et al. 2015). At GALAXIES, the beam size was 30x80 microns, incident energy was 10 keV and typical count rates were 70-150 counts/s. The emission signal was maximized by directing incident radiation through the diamond and collecting spectra at an angle of approximately 10° minimizing the path through the beryllium gasket.

T-SMS experiments were conducted at pressures up to 85 GPa using beamline 16-ID-D of the APS. Kirkpatrick-Baez mirrors were used to focus the X-ray beam to 30x40 μm. The storage

ring was operated in standard-mode with 24 bunches separated by 153 ns. Data were collected between 14 and 130 ns after excitation. Measurements were taken both with and without a 0.5-μm thick $^{57}$Fe-enriched stainless steel foil as a reference. Sample count rates at high pressure were 30-150 counts/s and spectra were typically collected for 30-60 minutes. At ambient pressure, both T-SMS and MS give consistent results (Figure 1, Tables 1-2).

E-SMS experiments were conducted at pressures up to 91 GPa at beamline ID18 of the European Synchrotron Radiation Facility (ESRF) (Rüffer and Chumakov 1996; Potapkin et al. 2012). The synchrotron beam was focused to 9x14 μm and monochromatized to a bandwidth of ~5.5 neV at the $^{57}$Fe resonant energy by a $^{57}FeBO_3$ single crystal. The crystal monochromator was oscillated in a sinusoidal mode over +/- 5 mm/s to provide a range of energies for absorption measurements via the Doppler effect. Source velocity was calibrated with an α-Fe foil. The linewidth and center shift of the source were verified before and after each measurement with $K_2Mg^{57}Fe(CN)_6$ standard.

## 3. Results

Glass samples were compressed without heating to maximum pressures up to 91 GPa. At ambient conditions, the glass is honey-brown and translucent, but darkens with pressure, becoming black and opaque by 34 GPa (Figure 2). Pressure-induced color change of $(Mg_{0.8}Fe_{0.2})SiO_3$ enstatite-composition glass was determined by optical absorption spectroscopy to occur from ~15-50 GPa (Murakami et al. 2014). An analogous color-change in crystalline samples is known to be associated with the garnet-perovskite transition (O'Neill and Jeanloz 1994; Kesson et al. 1995; Dorfman et al. 2012) but is not observed in cold-compressed almandine

to pressures above 1 Mbar (Dorfman et al. 2012). This change in optical properties decreases radiative thermal conductivity of Fe-bearing silicates in the mantle and may be associated with changes in electronic configuration (Murakami et al. 2014).

### 3. 1. X-ray emission spectroscopy

The observed Fe Kβ X-ray emission spectrum at ambient conditions is composed of a main $K\beta_{1,3}$ peak and a well-resolved lower-energy satellite Kβ' peak and is consistent with iron entirely in the high spin state (Figure 3). Up to 66 GPa in almandine glass, the Kβ' peak intensity continuously decreases and breadth increases (Figure 3). These changes may be due to either a gradual spin-pairing transition or pressure-induced broadening effects (Gu et al. 2012; Mao et al. 2014; Murakami et al. 2014).

Distinguishing between a gradual spin transition and spectral broadening depends on quantitative comparison with reference spectra. Several methods have been proposed for quantifying spin crossovers (Kantor et al. 2006; Vankó et al. 2006; Mao et al. 2014) and each may result in a different interpretation of the data. Simple peak-fitting techniques do not adequately model the Kβ spectrum due to the complexity of the energy multiplets from which the broader features are composed (Vankó et al. 2006). Instead, the spin state is derived from an integrated difference between spectra and reference high- and low-spin standard spectra. Relevant standards are keys to this method. Spectral differences can be due to differences in instrument resolution, crystallographic environment, and stress conditions as well as spin state, so these confounding factors must be minimized between standards and experiments (De Groot 2001; Vankó et al. 2006; Mao et al. 2014). A modification of the integrated difference technique

was recently proposed to minimize the effects of pressure-induced broadening (Mao et al. 2014). Difference spectra are summed such that negative differences at Kβ' are offset by positive differences in the shoulder between Kβ' and $K\beta_{1,3}$. This integrated relative difference (IRD) method was suggested to better model pressure-induced spin transitions both in (Mg,Fe)O ferropericlase and in Fe-bearing silicate glass (Mao et al. 2014).

The IRD analysis was applied to the almandine glass XES using as references (Mg,Fe)O from Lin et al. (2010) and the ambient-pressure glass spectrum. No significant difference is observed between the glass at 1 bar and (Mg,Fe)O at 1 bar. IRD at high pressure relative to either high-spin standard is identical within symbol size. Between 1 bar and the first high-pressure measurement at 9 GPa, a decrease in total spin moment begins. Total spin moment decreases gradually to ~80% of the high-spin standard by 27 GPa (Figure 3). At higher pressures up to 66 GPa there is no significant further change in spin. The gradual change in the spectrum above 27 GPa reflects only broadening due to pressure and/or differential stress.

In previous work on silicate glass at high pressure, analysis by the integrated absolute difference (IAD) method of Vankó et al. (2006) showed a gradual spin transition (Gu et al. 2012) while the IRD method showed only broadening (Mao et al. 2014). Analysis of our spectra with the IAD method also produces an apparent gradual loss of spin moment over the entire pressure range (Supplementary Figure 1). We thus confirm that the IRD analysis removes pressure-induced broadening and reduces the apparent change in spin relative to the IAD analysis, but we still observe partial loss of spin moment. The spin change can be linked to a valence state and site using Mössbauer spectroscopy.

## 3. 2. Synchrotron Mössbauer spectroscopy

Synchrotron Mössbauer spectroscopy was performed on almandine glass at high pressures in both energy- and time-domain modes. E-SMS (Figure 4) and T-SMS spectra (Supplementary Figure 2) evolve continuously with pressure. The major feature in E-SMS spectra is the asymmetrical doublet identified as $Fe^{2+}$. With compression the $Fe^{2+}$ doublet broadens and becomes increasingly asymmetrical. Pressure-induced changes in the $Fe^{2+}$ doublet are consistent with previous E-SMS measurements of $Fe^{2+}$-rich glasses with compositions $(Mg_{0.8}Fe_{0.2})SiO_3$ and $(Mg_{0.823}Fe_{0.135})(Al_{0.057}Si_{0.982})O_3$ (Murakami et al. 2014; Prescher et al. 2014). The small shoulder observed between the $Fe^{2+}$ lines (Figure 4) is identified as one leg of the $Fe^{3+}$ doublet. At higher pressures, a shoulder appears at higher velocity on the $Fe^{2+}$ doublet.

T-SMS spectra (Supplementary Figure 2) at low pressure have a sharp beat at ~60 ns and a broad decay after ~100 ns. At higher pressures, the beat shifts with pressure to faster times and becomes less distinct. Above 26 GPa, another small beat appears at ~80 ns. Despite differences in $Fe^{3+}/\Sigma Fe$ and total iron content, qualitatively similar spectra were observed at high pressure in $(Mg_{0.80}Fe_{0.20})SiO_3$ (~10% $Fe^{3+}$) and $(Mg_{0.75}Fe_{0.20}Al_{0.10}Si_{0.95})O_3$ (~35% $Fe^{3+}$) glasses by Gu et al. (2012) and $(Mg_{0.79}Fe_{0.10}Al_{0.10}Si_{0.96})O_3$ (78% $Fe^{3+}$) glass by Mao et al. (2014). However, starting from 17 GPa and increasing with pressure in the almandine glass studied here, resonant intensity is observed at ~110 ns. Neither previous study reports this structure, either due to difference in electronic states or effective sample thickness.

Modeling Mössbauer spectra of glasses is challenging due to the range of coordination environments and site geometries in a disordered structure. A simple two-site model with a distribution over IS or QS cannot fit the asymmetry observed in E-SMS and the complex

structure in T-SMS. An asymmetrical $Fe^{2+}$ doublet is observed in silicate glasses due to a range of coordination environments (Mao et al. 1973; Alberto et al. 1996). For glasses at both ambient conditions (Alberto et al. 1996; Lagarec and Rancourt 1997) and high pressures (Prescher et al. 2014), a correlated distribution over both IS and QS fits the asymmetrical $Fe^{2+}$ doublet (Supplementary Figure 3). E-SMS data in this study were analyzed using the correlated distribution model of Lagarec and Rancourt (1997) implemented for fitting E-SMS spectra in MossA software (Prescher et al. 2012). The correlated distribution for $Fe^{2+}$ can also be modeled with a pair of doublets of approximately equal intensity, one representing low-IS, low-QS and the other high-IS, high-QS (Supplementary Figure 3) (Virgo and Mysen 1985; Jayasuriya et al. 2004). T-SMS data in this study were analyzed using a paired $Fe^{2+}$ doublet model with fixed weighting in the CONUSS software package (Sturhahn 2000). T-SMS fits with a pair of doublets for $Fe^{2+}$ are consistent with observed E-SMS spectra (Supplementary Figure 2). $Fe^{3+}$ doublets are not fully resolved but assumed to be symmetric as previously observed at ambient pressure (Virgo and Mysen 1985) and high pressure (Prescher et al. 2014).

Our results demonstrate consistent pressure-dependence of Mössbauer parameters in three separate compression experiments with two SMS techniques (Figure 5, Tables 1-2). Observed Mössbauer parameters for the $Fe^{2+}$ doublet(s) at all conditions studied are consistent with previous observations of high-spin $Fe^{2+}$ in glasses (Dyar 1985; Virgo and Mysen 1985; Burkhard 2000), with average QS of 2.0-2.3 mm/s and IS of 0.8-1.1 mm/s. The QS of high-spin $Fe^{2+}$ increases slightly from 1 bar to 30 GPa and then slightly decreases up to the maximum pressure of 91 GPa. The IS of high-spin $Fe^{2+}$ decreases with pressure. The most significant change in the $Fe^{2+}$ component is an increase in the correlated broadening parameter related to the covariance of

QS and IS, ρ, particularly between 1 bar and ~40 GPa. In T-SMS fits, the increase in correlated broadening is modeled as a divergence of both QS and IS of two high-spin $Fe^{2+}$ doublets. The weight of the high-spin $Fe^{2+}$ component does not change significantly. If the change in spin state indicated by XES corresponds to a high-to-low spin transition in $Fe^{2+}$, we would expect a decrease in QS of the $Fe^{2+}$ site, as for the high-to-low spin transition in $Fe^{2+}$ in bridgmanite (Hsu et al. 2010), but this is not observed. Our data also do not support pressure-induced growth of an intermediate spin $Fe^{2+}$ component with parameters as reported by Murakami et al. (2014). The broadening of the $Fe^{2+}$ doublet could be interpreted as a gradual transition of half of the $Fe^{2+}$ component to intermediate spin below ~40 GPa. This is consistent with the total spin moment measured by XES, but unlikely as there is no obvious reason why the spin transition would stop, incomplete, at ~40 GPa.

Observations of the $Fe^{3+}$ component(s) are consistent with a high-to-low spin transition. At pressures >30 GPa, the values of QS for the $Fe^{3+}$ site are 1.7-2.0 mm/s. These values are outside the range of previous observations for high-spin $Fe^{3+}$ at ambient conditions (Figures 5-6) (Dyar 1985; Virgo and Mysen 1985; Burkhard 2000) and similar to previous observations of low-spin $Fe^{3+}$-bearing compounds (Greenwood and Gibb 1971; Pasternak et al. 2002). Moreover, both the weight of the $Fe^{3+}$ component, ~20% of the total Fe, and the pressure at which the $Fe^{3+}$ shoulder completes its shift, ~30 GPa, match the decrease in spin moment observed in XES data (Figure 3). A high-to-low spin transition in $Fe^{3+}$ should be observed as a decrease in the intensity of the high-spin doublet and corresponding growth of the low-spin doublet with lower IS and higher QS (Pasternak et al. 2002). We have thus chosen a model with two $Fe^{3+}$ doublets, although these two doublets are not fully resolved in our MS data. We are also unable to resolve

288 the minimum pressure at which the low-spin $Fe^{3+}$ appears, but at 15 GPa ~30% of the $Fe^{3+}$ is in
289 the low-spin state. The high- and low-spin doublets coexist over a wider pressure range in the
290 glass sample loaded in NaCl vs. Ne medium. This suggests that differential stress may result in a
291 broader spin transition, as reported in (Mg,Fe)O (Lin et al. 2009).

292 Previous Mössbauer studies of silicate glasses found generally similar QS and IS values
293 and changes with pressure as in our study (Figure 6). QS and IS for all sites in the almandine
294 glass are similar to those constrained by previous E-SMS studies on Fe-bearing silicate glasses at
295 high pressures (Murakami et al. 2014; Prescher et al. 2014). Studies using both E-SMS and T-
296 SMS techniques on a wide range of compositions have found an increase in QS of $Fe^{2+}$ at
297 pressures up to 20-40 GPa (Gu et al. 2012; Mao et al. 2014; Murakami et al. 2014; Prescher et al.
298 2014). A similar QS of high-pressure $Fe^{3+}$ was observed in $Fe^{3+}$-rich glass studied by Prescher et
299 al. (2014) and Gu et al. (2012), but not by Mao et al. (2014). IS of $Fe^{2+}$ was observed to decrease
300 with pressure in both previous E-SMS studies (Murakami et al. 2014; Prescher et al. 2014).
301 However, previous studies have offered different interpretations of these observations: no spin
302 transition (Mao et al. 2014; Prescher et al. 2014), a gradual high-to-low spin transition in
303 $Fe^{3+}$ (Gu et al. 2012) or a high-to-intermediate spin transition in $Fe^{2+}$ (Murakami et al. 2014). In
304 addition to differences in composition between these studies, differences in interpretation of
305 Mössbauer parameters are due to details of E-SMS and T-SMS fitting and availability and
306 interpretation of XES data.

307 ## 4. Discussion

The multiple techniques used in this study enable us to provide a strong constraint on the pressure-dependence of spin states of Fe in almandine glass. Optical properties, XES, and Mössbauer parameters of $Fe^{3+}$ all exhibit changes between 1 bar and ~30 GPa. These results support a gradual, complete transition of $Fe^{3+}$ in almandine glass from high to low spin and no detectable change in spin state of $Fe^{2+}$.

This transition in $Fe^{3+}$ could not be reliably identified in previous studies that did not use multiple experimental techniques. Fitting T-SMS spectra alone suffers from non-unique constraints on Mössbauer parameters. Gu et al. (2012) model spectra using a pair of $Fe^{2+}$ doublets similar to those in this study, but their strong change in intensity with pressure is inconsistent with other studies of silicate glasses and may be an artifact of non-unique fitting. Mao et al. (2014) restrict their model to two sites of constant intensity, one each for high spin $Fe^{2+}$ and $Fe^{3+}$, but their modeled energy-domain spectra exhibit varying degrees of asymmetry which is not explained. The previous E-SMS study of $Fe^{3+}$-rich silicate glass (Prescher et al. 2014) finds a similar increase in QS as in our observations of almandine glass (Figure 6). The doublet identified at pressures above 20 GPa as intermediate spin $Fe^{2+}$ by Murakami et al. (2014) is consistent with $Fe^{3+}$ at high pressures in this study and Prescher et al. (2014) (Figure 6). However, previous studies using the E-SMS technique were not combined with XES measurements and thus were unable to relate changes in Mössbauer parameters to changes in total spin moment.

While our results and previous studies cover a wide range of compositions, all time- or energy-domain Mössbauer studies of glass to date consistently find that there is no sharp transition in spin or structure with pressure up to 126 GPa (Gu et al. 2012; Mao et al. 2014;

330 Murakami et al. 2014; Prescher et al. 2014). Almandine glass is much richer in Fe than the
331 compositions studied in other work; this may promote a spin transition at relatively lower
332 pressures (Prescher et al. 2014). The sharp spin transition observed in XES data by Nomura et al.
333 (2011) in $(Mg_{0.95}Fe_{0.05})SiO_3$ glass at 76 GPa is inconsistent with this and other studies. Similar
334 experimental methods were used by Nomura et al. (2011) and more recent studies, and thus these
335 results remain unexplained and unreplicated.

336 A spin transition in $Fe^{3+}$ in silicate glasses is analogous to transitions in crystalline Fe-
337 bearing silicates. In bridgmanite, $Fe^{3+}$ in the 6-fold-coordinated B-site is predicted theoretically to
338 undergo a spin transition at 40-70 GPa, but both $Fe^{3+}$ and $Fe^{2+}$ in the 8-fold-coordinated A-site
339 remain high-spin throughout the lower mantle pressure range (Hsu et al. 2010, 2011). Spin
340 transitions in $Fe^{3+}$ have been observed at various pressures in the range of 13-70 GPa by several
341 experimental studies of bridgmanite (e.g. Catalli et al. 2010, 2011; Mao et al. 2011; Lin et al.
342 2012) and other $Fe^{3+}$-bearing perovskites (Xu et al. 2001; Pasternak et al. 2002; Rozenberg et al.
343 2005). In addition, a discontinuity in volumetric compression was attributed to a spin transition in
344 6-fold-coordinated $Fe^{3+}$ in andradite garnet at 60-70 GPa (Friedrich et al. 2014). No spin
345 transition has been observed in 8-fold-coordinated $Fe^{2+}$ in pyrope-almandine garnets, but studies
346 of the equation of state and electronic configuration of these garnets have only reached ~30 GPa
347 (e.g. Mao et al. 2013).

348 In silicate glass, $Fe^{3+}$ and $Fe^{2+}$ both occupy a range of coordination environments. In
349 $MgSiO_3$ glasses, the average coordination number is 6 in the Mg-site and 4 in the Si-site, and
350 these averages increase with pressure (Funamori et al. 2004). The average coordination of Si in
351 $SiO_2$ glass has been suggested by experiments and simulations to increase stepwise or

continuously with compression (e.g. Meade et al. 1992). While compression alone generally increases QS while decreasing IS (e.g. Pasternak et al. 2002; Kantor et al. 2006), increasing coordination of Fe increases both QS and IS (Dyar et al. 2006). Observed increases in QS of $Fe^{2+}$ with pressure in silicate glasses have been interpreted to show densification by increasing coordination number to 8-12 (Mao et al. 2014). However, in the almandine glass we observe not only a slight increase in QS but an increase in broadening of the $Fe^{2+}$ site. This doublet represents a superposition of multiple sites with different coordination which cannot be resolved in the glass. Pressure-induced changes in Mössbauer parameters of $Fe^{2+}$ do not depend on pressure medium and are thus unlikely to be due to non-hydrostatic stress. The increase in correlated broadening of the $Fe^{2+}$ doublet with compression (Figure 7) suggests a broadening of the range of coordination environments. The population of $Fe^{2+}$ with highest QS and IS, in higher coordination, would thus increase with pressure without completely replacing $Fe^{2+}$ with lowest QS and IS, in 4- to 6-fold coordination.

## 5. Implications

A sharp spin transition in iron in silicate glasses would suggest a discontinuity in the properties of melt in the lower mantle or deep in a magma ocean; conversely, no sharp spin transition in the glass supports a smooth variation of the properties of silicate melts with depth. This study represents the first high-pressure examination of almandine glass and the first combination of energy- and time-domain synchrotron Mössbauer spectra and X-ray emission spectra techniques at high pressure for any silicate glass. All methods consistently support a broad spin transition in $Fe^{3+}$ between 1 bar and ~30 GPa without an abrupt discontinuity. Our

observations differ from the previous observation of a sharp transition in Fe-bearing glass and accompanying changes in solid-melt iron partitioning. We would expect that in a melt of almandine composition, effects of temperature may further broaden the spin transition to a greater range than the ~30-GPa interval observed in the glass. Our study supports the expectation that spin transitions in iron-bearing silicate melts in Earth's mantle should be broad with respect to transitions in their crystalline counterparts. No discontinuities are expected to occur under compression in the density or transport properties of Fe-rich mantle melts.

In addition, the bonding of $Fe^{2+}$ shifts to a broader range of coordination numbers over 1 bar to ~60 GPa. These changes are accompanied by a change in color from transparent to black, suggesting a pressure-induced reduction in radiative thermal conductivity in Fe-rich silicate liquids. This increasing diversity of bonding styles may have important implications for transport properties of the glass or melt network in the Earth's deep mantle or early magma ocean.

## Acknowledgements

We thank L. Dubrovinsky, I. Kupenko, S.-H. Shim, and C. Gu for helpful discussions about experiment design and interpretation. J. Wicks, G. J. Finkelstein and C. V. Stan made suggestions that improved this manuscript. G. Poirier provided help with electron microscopy of starting materials. We acknowledge the usage of PRISM Imaging and Analysis Center which is supported in part by the NSF MRSEC program through the Princeton Center for Complex Materials (grant DMR-0819860). J. Delaney assisted with chemical analyses at the Rutgers University microprobe facility. E-SMS experiments were performed on the ID18 beamline at the European Synchrotron Radiation Facility (ESRF), Grenoble, France. We are grateful to I.

Kupenko at ERSF for providing assistance in using beamline ID18. J. Jacobs assisted with gas loading at the ESRF. T-SMS experiments were performed at the High Pressure Collaborative Access Team (HPCAT), Sector 16 of the Advanced Photon Source (APS), Argonne National Laboratory. HPCAT operations are supported by DOE-NNSA under Award No. DE-NA0001974 and DOE-BES under Award No. DE-FG02-99ER45775, with partial instrumentation funding by NSF. The Advanced Photon Source is a U.S. Department of Energy (DOE) Office of Science User Facility operated for the DOE Office of Science by Argonne National Laboratory under Contract No. DE-AC02-06CH11357. Use of the COMPRES-GSECARS gas loading system was supported by COMPRES under NSF Cooperative Agreement EAR 11-57758 and by GSECARS through NSF grant EAR-1128799 and DOE grant DE-FG02-94ER14466. We acknowledge SOLEIL for provision of synchrotron radiation facilities for XES (Proposal ID 20130184) and we would like to thank B. Lassalle and J. Ablett for assistance in using beamline GALAXIES.

## References

Akahama, Y., and Kawamura, H. (2006) Pressure calibration of diamond anvil Raman gauge to 310 GPa. Journal of Applied Physics, 100, 043516–4.

Alberto, H.V., Pinto da Cunha, J.L., Mysen, B.O., Gil, J.M., and Ayres de Campos, N. (1996) Analysis of Mössbauer spectra of silicate glasses using a two-dimensional Gaussian distribution of hyperfine parameters. Journal of Non-Crystalline Solids, 194, 48–57.

Andrault, D., Petitgirard, S., Nigro, G.L., Devidal, J.-L., Veronesi, G., Garbarino, G., and Mezouar, M. (2012) Solid-liquid iron partitioning in Earth's deep mantle. Nature, 487, 354–357.

Badro, J., Fiquet, G., Guyot, F., Rueff, J.-P., Struzhkin, V.V., Vankó, G., and Monaco, G. (2003) Iron Partitioning in Earth's Mantle: Toward a Deep Lower Mantle Discontinuity. Science, 300, 789–791.

Badro, J., Rueff, J.-P., Vanko, G., Monaco, G., Fiquet, G., and Guyot, F. (2004) Electronic Transitions in Perovskite: Possible Nonconvecting Layers in the Lower Mantle. Science, 305, 383–386.

Burkhard, D.J.M. (2000) Iron-bearing silicate glasses at ambient conditions. Journal of Non-Crystalline Solids, 275, 175–188.

Catalli, K., Shim, S.-H., Prakapenka, V.B., Zhao, J., Sturhahn, W., Chow, P., Xiao, Y., Liu, H., Cynn, H., and Evans, W.J. (2010) Spin state of ferric iron in $MgSiO_3$ perovskite and its effect on elastic properties. Earth and Planetary Science Letters, 289, 68–75.

Catalli, K., Shim, S.-H., Dera, P., Prakapenka, V.B., Zhao, J., Sturhahn, W., Chow, P., Xiao, Y., Cynn, H., and Evans, W.J. (2011) Effects of the $Fe^{3+}$ spin transition on the properties of aluminous perovskite—New insights for lower-mantle seismic heterogeneities. Earth and Planetary Science Letters, 310, 293–302.

Cottrell, E., and Kelley, K.A. (2011) The oxidation state of Fe in MORB glasses and the oxygen fugacity of the upper mantle. Earth and Planetary Science Letters, 305, 270–282.

De Groot, F. (2001) High-resolution X-ray emission and X-ray absorption spectroscopy. Chemical Reviews, 101, 1779–1808.

Dorfman, S.M., Shieh, S.R., Meng, Y., Prakapenka, V.B., and Duffy, T.S. (2012) Synthesis and equation of state of perovskites in the $(Mg, Fe)_3Al_2Si_3O_{12}$ system to 177 GPa. Earth and Planetary Science Letters, 357–358, 194–202.

Dunlap, R.A., and McGraw, J.D. (2007) A Mössbauer effect study of Fe environments in impact glasses. Journal of Non-Crystalline Solids, 353, 2201–2205.

Dyar, M.D. (1985) A review of Moessbauer data on inorganic glasses; the effects of composition on iron valency and coordination. American Mineralogist, 70, 304–316.

Dyar, M.D., Agresti, D.G., Schaefer, M.W., Grant, C.A., and Sklute, E.C. (2006) Mössbauer spectroscopy of Earth and planetary materials. Annual Review of Earth and Planetary Sciences, 34, 83–125.

Fei, Y., Zhang, L., Corgne, A., Watson, H., Ricolleau, A., Meng, Y., and Prakapenka, V. (2007) Spin transition and equations of state of (Mg, Fe)O solid solutions. Geophysical Research Letters, 34, L17307.

Friedrich, A., Winkler, B., Morgenroth, W., Ruiz-Fuertes, J., Koch-Müller, M., Rhede, D., and Milman, V. (2014) Pressure-induced spin collapse of octahedrally coordinated $Fe^{3+}$ in $Ca_3Fe_2[SiO_4]_3$ from experiment and theory. Physical Review B, 90, 094105.

Funamori, N., Yamamoto, S., Yagi, T., and Kikegawa, T. (2004) Exploratory studies of silicate melt structure at high pressures and temperatures by in situ X-ray diffraction. Journal of Geophysical Research: Solid Earth, 109, B03203.

Geiger, C.., Newton, R.., and Kleppa, O.. (1987) Enthalpy of mixing of synthetic almandine-grossular and almandine-pyrope garnets from high-temperature solution calorimetry. Geochimica et Cosmochimica Acta, 51, 1755–1763.

Greenwood, N.N., and Gibb, T.C. (1971) Low-spin Iron(II) and Iron(III) Complexes. In Mössbauer Spectroscopy pp. 169–193. Springer Netherlands.

Gu, C., Catalli, K., Grocholski, B., Gao, L., Alp, E., Chow, P., Xiao, Y., Cynn, H., Evans, W.J., and Shim, S.-H. (2012) Electronic structure of iron in magnesium silicate glasses at high pressure. Geophysical Research Letters, 39.

Hsu, H., Umemoto, K., Blaha, P., and Wentzcovitch, R.M. (2010) Spin states and hyperfine interactions of iron in (Mg,Fe)$SiO_3$ perovskite under pressure. Earth and Planetary Science Letters, 294, 19–26.

Hsu, H., Blaha, P., Cococcioni, M., and Wentzcovitch, R.M. (2011) Spin-State Crossover and Hyperfine Interactions of Ferric Iron in $MgSiO_3$ Perovskite. Physical Review Letters, 106, 118501.

Jackson, J.M., Sturhahn, W., Shen, G., Zhao, J., Hu, M.Y., Errandonea, D., Bass, J.D., and Fei, Y. (2005) A synchrotron Mössbauer spectroscopy study of (Mg,Fe)$SiO_3$ perovskite up to 120 GPa. American Mineralogist, 90, 199–205.

Jayasuriya, K.D., O'Neill, H.S.C., Berry, A.J., and Campbell, S.J. (2004) A Mössbauer study of the oxidation state of Fe in silicate melts. American Mineralogist, 89, 1597–1609.

Kantor, I., Dubrovinsky, L., McCammon, C., Steinle-Neumann, G., Kantor, A., Skorodumova, N., Pascarelli, S., and Aquilanti, G. (2009) Short-range order and Fe clustering in $Mg_{1-x}Fe_xO$ under high pressure. Physical Review B, 80, 014204.

Kantor, I.Y., Dubrovinsky, L.S., and McCammon, C.A. (2006) Spin crossover in (Mg,Fe)O: A Mössbauer effect study with an alternative interpretation of x-ray emission spectroscopy data. Physical Review B, 73, 100101.

Kesson, S.E., Fitzgerald, J.D., Shelley, J.M.G., and Withers, R.L. (1995) Phase relations, structure and crystal chemistry of some aluminous silicate perovskites. Earth and Planetary Science Letters, 134, 187–201.

Labrosse, S., Hernlund, J.W., and Coltice, N. (2007) A crystallizing dense magma ocean at the base of the Earth's mantle. Nature, 450, 866–869.

Lagarec, K., and Rancourt, D.G. (1997) Extended Voigt-based analytic lineshape method for determining N-dimensional correlated hyperfine parameter distributions in Mössbauer spectroscopy. Nuclear Instruments and Methods in Physics Research Section B: Beam Interactions with Materials and Atoms, 129, 266–280.

Lee, C. -t. A., Luffi, P., Hoink, T., Li, J., Dasgupta, R., and Hernlund, J. (2010) Upside-down differentiation and generation of a "primordial" lower mantle. Nature, 463, 930–933.

Lin, J.-F., and Tsuchiya, T. (2008) Spin transition of iron in the Earth's lower mantle. Physics of the Earth and Planetary Interiors, 170, 248–259.

Lin, J.-F., Vankó, G., Jacobsen, S.D., Iota, V., Struzhkin, V.V., Prakapenka, V.B., Kuznetsov, A., and Yoo, C.-S. (2007) Spin Transition Zone in Earth's Lower Mantle. Science, 317, 1740 –1743.

Lin, J.-F., Wenk, H.-R., Voltolini, M., Speziale, S., Shu, J., and Duffy, T.S. (2009) Deformation of lower-mantle ferropericlase (Mg,Fe)O across the electronic spin transition. Physics and Chemistry of Minerals, 36, 585–592.

Lin, J.-F., Mao, Z., Jarrige, I., Xiao, Y., Chow, P., Okuchi, T., Hiraoka, N., and Jacobsen, S.D. (2010) Resonant X-ray emission study of the lower-mantle ferropericlase at high pressures. American Mineralogist, 95, 1125–1131.

Lin, J.-F., Alp, E.E., Mao, Z., Inoue, T., McCammon, C., Xiao, Y., Chow, P., and Zhao, J. (2012) Electronic spin states of ferric and ferrous iron in the lower-mantle silicate perovskite. American Mineralogist, 97, 592–597.

Mao, H.K., Virgo, D., and Bell, P.M. (1973) Analytical Study of the Orange Lunar Soil Returned by the Apollo 17 Astronauts. In Year Book Carnegie Institution of Washington pp. 631–638. Carnegie Institution of Washington, Washington, D.C.

Mao, H. -k., Xu, J., and Bell, P.M. (1986) Calibration of the Ruby Pressure Gauge to 800 kbar Under Quasi-Hydrostatic Conditions. Journal of Geophysical Research, 91, 4673–4676.

Mao, Z., Lin, J.F., Scott, H.P., Watson, H.C., Prakapenka, V.B., Xiao, Y., Chow, P., and McCammon, C. (2011) Iron-rich perovskite in the Earth's lower mantle. Earth and Planetary Science Letters, 309, 179–184.

Mao, Z., Lin, J.-F., Huang, S., Chen, J., Xiao, Y., and Chow, P. (2013) Synchrotron Mössbauer study of Fe-bearing pyrope at high pressures and temperatures. American Mineralogist, 98, 1146–1152.

Mao, Z., Lin, J.-F., Yang, J., Wu, J., Watson, H.C., Xiao, Y., Chow, P., and Zhao, J. (2014) Spin and valence states of iron in Al-bearing silicate glass at high pressures studied by synchrotron Mössbauer and X-ray emission spectroscopy. American Mineralogist, 99, 415–423.

518 Mattila, A., Rueff, J.-P., Badro, J., Vankó, G., and Shukla, A. (2007) Metal-ligand interplay in
519 strongly correlated oxides: A parametrized phase diagram for pressure-induced spin
520 transitions. Physical Review Letters, 98, 196404.

521 Meade, C., Hemley, R.J., and Mao, H.K. (1992) High-pressure x-ray diffraction of $SiO_2$ glass.
522 Physical Review Letters, 69, 1387–1390.

523 Mitsui, T., Hirao, N., Ohishi, Y., Masuda, R., Nakamura, Y., Enoki, H., Sakaki, K., and Seto, M.
524 (2009) Development of an energy-domain $^{57}$Fe-Mössbauer spectrometer using
525 synchrotron radiation and its application to ultrahigh-pressure studies with a diamond
526 anvil cell. Journal of Synchrotron Radiation, 16, 723–729.

527 Muñoz Ramo, D., and Stixrude, L. (2014) Spin crossover in $Fe_2SiO_4$ liquid at high pressure.
528 Geophysical Research Letters, 41.

529 Murakami, M., Goncharov, A.F., Hirao, N., Masuda, R., Mitsui, T., Thomas, S.-M., and Bina,
530 C.R. (2014) High-pressure radiative conductivity of dense silicate glasses with potential
531 implications for dark magmas. Nature Communications, 5.

532 Mysen, B.O. (2006) The structural behavior of ferric and ferrous iron in aluminosilicate glass
533 near meta-aluminosilicate joins. Geochimica et Cosmochimica Acta, 70, 2337–2353.

534 Nomura, R., Ozawa, H., Tateno, S., Hirose, K., Hernlund, J., Muto, S., Ishii, H., and Hiraoka, N.
535 (2011) Spin crossover and iron-rich silicate melt in the Earth's deep mantle. Nature, 473,
536 199–202.

537 O'Neill, B., and Jeanloz, R. (1994) $MgSiO_3$-$FeSiO_3$-$Al_2O_3$ in the Earth's lower mantle:
538 Perovskite and garnet at 1200 km depth. Journal of Geophysical Research, 99, 19,901–
539 19,915.

540 Pasternak, M.P., Xu, W.M., Rozenberg, G.K., and Taylor, R.D. (2002) Electronic, Magnetic and
541 Structural Properties of the $RFeO_3$ Antiferromagnetic-Perovskites at Very High Pressures.
542 In Symposium D – Perovskite Materials Vol. 718.

543 Peng, G., Wang, X., Randall, C.R., Moore, J.A., and Cramer, S.P. (1994) Spin selective x-ray
544 absorption spectroscopy: Demonstration using high resolution Fe Kβ fluorescence.
545 Applied Physics Letters, 65, 2527–2529.

546 Potapkin, V., Chumakov, A.I., Smirnov, G.V., Celse, J.-P., Rüffer, R., McCammon, C., and
547 Dubrovinsky, L. (2012) The $^{57}$Fe Synchrotron Mössbauer Source at the ESRF. Journal of
548 Synchrotron Radiation, 19, 559–569.

549 Prescher, C., McCammon, C., and Dubrovinsky, L. (2012) MossA: a program for analyzing
550 energy-domain Mössbauer spectra from conventional and synchrotron sources. Journal of
551 Applied Crystallography, 45, 329–331.

552 Prescher, C., Weigel, C., McCammon, C., Narygina, O., Potapkin, V., Kupenko, I., Sinmyo, R.,
553 Chumakov, A.I., and Dubrovinsky, L. (2014) Iron spin state in silicate glass at high
554 pressure: Implications for melts in the Earth's lower mantle. Earth and Planetary Science
555 Letters, 385, 130–136.

556 Rivers, M., Prakapenka, V., Kubo, A., Pullins, C., Holl, C.M., and Jacobsen, S.D. (2008) The
557 COMPRES/GSECARS gas-loading system for diamond anvil cells at the Advanced
558 Photon Source. High Pressure Research, 28, 273–292.

559 Rossano, S., Behrens, H., and Wilke, M. (2007) Advanced analyses of $^{57}$Fe Mössbauer data of
560 alumino-silicate glasses. Physics and Chemistry of Minerals, 35, 77–93.

561 Rozenberg, G.K., Pasternak, M.P., Xu, W.M., Dubrovinsky, L.S., Carlson, S., and Taylor, R.D.
562 (2005) Consequences of pressure-instigated spin crossover in $RFeO_3$ perovskites; a
563 volume collapse with no symmetry modification. EPL (Europhysics Letters), 71, 228.

564 Rueff, J.-P., Kao, C.-C., Struzhkin, V.V., Badro, J., Shu, J., Hemley, R.J., and Mao, H.K. (1999)
565 Pressure-Induced High-Spin to Low-Spin Transition in FeS Evidenced by X-Ray
566 Emission Spectroscopy. Physical Review Letters, 82, 3284.

567 Rueff, J.-P., Ablett, J.M., Céolin, D., Prieur, D., Moreno, T., Balédent, V., Lassalle-Kaiser, B.,
568 Rault, J.E., Simon, M., and Shukla, A. (2015) The GALAXIES beamline at the SOLEIL
569 synchrotron: inelastic X-ray scattering and photoelectron spectroscopy in the hard X-ray
570 range. Journal of Synchrotron Radiation, 22.

571 Rüffer, R., and Chumakov, A.I. (1996) Nuclear Resonance Beamline at ESRF. Hyperfine
572 Interactions, 97-98, 589–604.

573 Smirnov, G.V., van Bürck, U., Chumakov, A.I., Baron, A.Q.R., and Rüffer, R. (1997)
574 Synchrotron Mössbauer source. Physical Review B, 55, 5811–5815.

575 Speziale, S., Milner, A., Lee, V.E., Clark, S.M., Pasternak, M.P., and Jeanloz, R. (2005) Iron spin
576 transition in Earth's mantle. Proceedings of the National Academy of Sciences of the
577 United States of America, 102, 17918–17922.

578 Stixrude, L., and Karki, B. (2005) Structure and Freezing of $MgSiO_3$ Liquid in Earth's Lower
579 Mantle. Science, 310, 297–299.

580 Stixrude, L., de Koker, N., Sun, N., Mookherjee, M., and Karki, B.B. (2009) Thermodynamics of
581 silicate liquids in the deep Earth. Earth and Planetary Science Letters, 278, 226–232.

582 Sturhahn, W. (2000) CONUSS and PHOENIX: Evaluation of nuclear resonant scattering data.
583 Hyperfine Interactions, 125, 149–172.

584 Sturhahn, W., Jackson, J.M., and Lin, J.-F. (2005) The spin state of iron in minerals of Earth's
585 lower mantle. Geophysical Research Letters, 32, L12307.

Thomas, C.W., Liu, Q., Agee, C.B., Asimow, P.D., and Lange, R.A. (2012) Multi-technique equation of state for $Fe_2SiO_4$ melt and the density of Fe-bearing silicate melts from 0 to 161 GPa. Journal of Geophysical Research: Solid Earth, 117, B10206.

Tsuchiya, T., Wentzcovitch, R.M., da Silva, C.R., and de Gironcoli, S. (2006) Spin transition in magnesiowüstite in Earth's lower mantle. Physical Review Letters, 96, 198501.

Vankó, G., Neisius, T., Molnár, G., Renz, F., Karpati, S., Shukla, A., and de Groot, F.M.F. (2006) Probing the 3d spin momentum with X-ray emission spectroscopy: The case of molecular-spin transitions. The Journal of Physical Chemistry B, 110, 11647–11653.

Virgo, D., and Mysen, B.O. (1985) The structural state of iron in oxidized vs. reduced glasses at 1 atm: A $^{57}$Fe Mössbauer study. Physics and Chemistry of Minerals, 12, 65–76.

Williams, Q., and Garnero, E.J. (1996) Seismic Evidence for Partial Melt at the Base of Earth's Mantle. Science, 273, 1528–1530.

Woodland, A.B., and Ross, C.R. (1994) A crystallographic and Mössbauer spectroscopy study of $Fe_3^{2+}Al_2Si_3O_{12}$-$Fe_3^{2+}Fe_2^{3+}Si_3O_{12}$, (almandine-"skiagite") and $Ca_3Fe_2^{3+}Si_3O_{12}$-$Fe_3^{2+}Fe_2^{3+}Si_3O_{12}$ (andradite-"skiagite") garnet solid solutions. Physics and Chemistry of Minerals, 21, 117–132.

Xu, W.M., Naaman, O., Rozenberg, G.K., Pasternak, M.P., and Taylor, R.D. (2001) Pressure-induced breakdown of a correlated system: The progressive collapse of the Mott-Hubbard state in $RFeO_3$. Physical Review B, 64, 094411.

## List of figure captions

Table 1: Mössbauer parameters observed by energy-domain Mössbauer spectroscopy for glass compressed in Ne or NaCl medium. QS=quadrupole splitting, IS=isomer shift, ρ=correlation parameter, FWHM=line full width at half maximum.

**Table 2**: Mössbauer parameters observed by time-domain Mössbauer spectroscopy for glass compressed in Ne medium. QS=quadrupole splitting, ΔIS=difference in isomer shift between $Fe^{2+}$ and $Fe^{3+}$ doublets, FWHM=full width at half maximum. ΔIS is given due to limited absolute reference constraint on IS. Starred parameters were fixed in fits. Fitting uncertainties for QS and IS are ~0.01 mm/s.

Figure 1: a) Conventional (energy-domain) and b) synchrotron Mössbauer (time-domain) spectra of almandine glass at 1 bar and 2-site fit (solid line). Residual for energy-domain fit is shown by gray dots in the upper part of the figure. $Fe^{2+}$ and $Fe^{3+}$ doublets are shown in dark and light gray, respectively.

Figure 2: Photomicrograph of opaque, black glass sample at 34 GPa in Ne medium with ruby ball.

Figure 3: XES spectra for almandine glass normalized to area and shifted to position of the main peak (Mao et al. 2014). Difference spectra below are relative to the low-spin (Mg,Fe)O reference (Lin et al. 2010). Inset: total spin moment calculated from XES spectra (black) and from weight of low-spin $Fe^{3+}$ component in E-SMS spectra (red). TSM for XES was determined from the

integrated relative difference (IRD) between spectra and high- and low-spin (Mg,Fe)O references (Lin et al. 2010).

Figure 4: Energy-domain synchrotron Mössbauer spectra for almandine glass in a neon pressure medium. Data are displayed as open circles. Curves are high-spin $Fe^{2+}$ doublet fit (blue), high-spin $Fe^{3+}$ doublet fit (pink), low-spin $Fe^{3+}$ doublet fit (red), baseline (gray) and total fit (black).

Figure 5: Observed Mössbauer parameters from almandine glass. $Fe^{2+}$ component is represented by two doublets in time-domain measurements (open symbols) and a single doublet with correlated quadrupole splitting and isomer shift in energy-domain measurements (filled symbols). Separate high- and low-spin $Fe^{3+}$ components are modeled in energy-domain measurements. a) Quadrupole splitting of each doublet. Triangles joined by lines represent the two $Fe^{2+}$ sites used to model the range of $Fe^{2+}$ environments in time-domain fits. b) Weight of each doublet. Two $Fe^{2+}$ doublets of equal weight are used for time-domain fits.

Figure 6: Quadrupole splitting vs. isomer shift for silicate and inorganic glasses derived from energy-domain Mössbauer spectroscopy. Literature values for glasses at ambient conditions are shown in small open black squares (Dyar 1985; Virgo and Mysen 1985; Burkhard 2000). Colors indicate Fe species identified at high pressure: dark blue=high-spin $Fe^{2+}$, light blue = intermediate spin $Fe^{2+}$, pink=high-spin $Fe^{3+}$, red= low-spin $Fe^{3+}$. Glasses at high pressures are shown with filled symbols (triangles=Prescher et al. (2014), diamonds=Murakami et al. (2014), circles= this study). Arrows indicate change observed with increasing pressure.

Figure 7: Correlation parameter of distribution of QS and IS in fits of $Fe^{2+}$ doublet. Solid symbols: compression in Ne medium. Open symbols: compression in NaCl medium.

**Table 1**

| | High spin $Fe^{2+}$ | | | | | | | |
|---|---|---|---|---|---|---|---|---|
| Pressure (GPa) | Weight (%) | QS (mm/s) | IS (mm/s) | ρ | | | | |
| Ambient | | | | | | | | |
| 0.0001 | 82(3) | 2.08(3) | 0.982(14) | 0.273 | | | | |
| Ne medium | | | | | | | | |
| 0.2 | 81(12) | 1.99(2) | 1.089(10) | 0.525 | | | | |
| 5 | 87(4) | 2.07(2) | 1.086(12) | 0.423 | | | | |
| 15 | 87(4) | 2.247(19) | 1.035(13) | 0.557 | | | | |
| 41 | 88(4) | 2.24(2) | 0.959(10) | 0.765 | | | | |
| 54 | 89(5) | 2.18(4) | 0.890(14) | 0.826 | | | | |
| NaCl medium | | | | | | | | |
| 7 | 87.6(1.9) | 2.05(2) | 1.066(9) | 0.339 | | | | |
| 18 | 84(3) | 2.319(14) | 1.036(12) | 0.491 | | | | |
| 30 | 85(5) | 2.30(3) | 0.99(2) | 0.682 | | | | |
| 42 | 84(5) | 2.26(3) | 0.94(2) | 0.785 | | | | |
| 57 | 86(6) | 2.20(4) | 0.86(3) | 0.773 | | | | |
| 70 | 84(6) | 2.13(4) | 0.86(4) | 0.967 | | | | |
| 91 | 86(5) | 2.05(3) | 0.81(3) | 0.859 | | | | |
| | High spin $Fe^{3+}$ | | | | Low spin $Fe^{3+}$ | | | |
| Pressure (GPa) | Weight (%) | QS (mm/s) | IS (mm/s) | FWHM (mm/s) | Weight (%) | QS (mm/s) | IS (mm/s) | FWHM (mm/s) |
| Ambient | | | | | | | | |
| 0.0001 | 18(3) | 1.23(11) | 0.39(5) | 0.63(13) | | | | |
| Ne medium | | | | | | | | |
| 0.2 | 19(8) | 1.18(9) | 0.43(5) | 0.58(12) | -- | -- | -- | -- |
| 5 | 13(6) | 1.20(18) | 0.46(10) | 0.53(15) | -- | -- | -- | -- |
| 15 | 9(3) | 0.74(13) | 0.57(5) | 0.36(16) | 4(4) | 1.74(10) | 0.48(5) | 0.2(2) |
| 41 | -- | -- | -- | -- | 12(4) | 1.82(7) | 0.36(3) | 0.33(10) |
| 54 | -- | -- | -- | -- | 11(4) | 1.83(6) | 0.35(3) | 0.36(13) |
| NaCl medium | | | | | | | | |
| 7 | 12.4(1.9) | 1.17(13) | 0.41(7) | 0.50(12) | -- | -- | -- | -- |
| 18 | 9.1(1.7) | 0.90(7) | 0.64(3) | 0.32(7) | 7(3) | 1.97(5) | 0.53(3) | 0.23(10) |
| 30 | 5(3) | 0.90(8) | 0.61(4) | 0.25(12) | 9(5) | 1.88(7) | 0.42(3) | 0.31(13) |
| 42 | 4(3) | 0.92(8) | 0.62(3) | 0.24(13) | 12(5) | 1.93(7) | 0.41(3) | 0.35(11) |
| 57 | 4(3) | 0.99(7) | 0.62(3) | 0.20(14) | 10(5) | 2.00(7) | 0.38(3) | 0.33(12) |
| 70 | -- | -- | -- | -- | 16(6) | 1.88(6) | 0.34(3) | 0.39(11) |
| 91 | -- | -- | -- | -- | 14(5) | 1.84(6) | 0.30(3) | 0.40(11) |

**Table 2**

| $Fe^{2+}$ | | | | | | | | |
|---|---|---|---|---|---|---|---|---|
| Pressure (GPa) | Weight (%) | QS (mm/s) | ΔIS (mm/s) | FWHM (mm/s) | Weight (%) | QS (mm/s) | ΔIS (mm/s) | FWHM (mm/s) |
| 0.0001 | 83 | 2.10 | 0.56 | 0.63 | | | | |
| 6 | 40* | 1.90 | 0.55 | 0.68 | 40* | 2.25 | 0.66 | 0.79 |
| 17 | 40* | 2.07 | 0.55 | 0.70 | 40* | 2.34 | 0.83 | 0.74 |
| 26 | 40* | 1.99 | 0.57 | 0.69 | 40* | 2.64 | 0.69 | 0.75 |
| 37 | 40* | 2.02 | 0.54 | 0.71 | 40* | 2.66 | 0.75 | 0.76 |
| 47 | 40* | 1.95 | 0.54 | 0.72 | 40* | 2.67 | 0.77 | 0.74 |
| 56 | 40* | 2.02 | 0.51 | 0.71 | 40* | 2.66 | 0.78 | 0.77 |
| 65 | 40* | 2.01 | 0.50 | 0.69* | 40* | 2.66 | 0.79 | 0.78* |
| 76 | 40* | 1.91 | 0.51 | 0.69 | 40* | 2.66 | 0.77 | 0.78 |
| 85 | 40* | 1.88 | 0.54 | 0.69* | 40* | 2.66 | 0.80 | 0.78* |

| $Fe^{3+}$ | | | |
|---|---|---|---|
| Pressure (GPa) | Weight (%) | QS (mm/s) | FWHM (mm/s) |
| 0.0001 | 17 | 1.17 | 0.77 |
| 6 | 20* | 1.14 | 0.64 |
| 17 | 20* | 1.58 | 0.63 |
| 26 | 20* | 1.72 | 0.59 |
| 37 | 20* | 1.81 | 0.54 |
| 47 | 20* | 1.81 | 0.53 |
| 56 | 20* | 1.84 | 0.51 |
| 65 | 20* | 1.83 | 0.48* |
| 76 | 20* | 1.77 | 0.48 |
| 85 | 20* | 1.77 | 0.48* |

# Figures

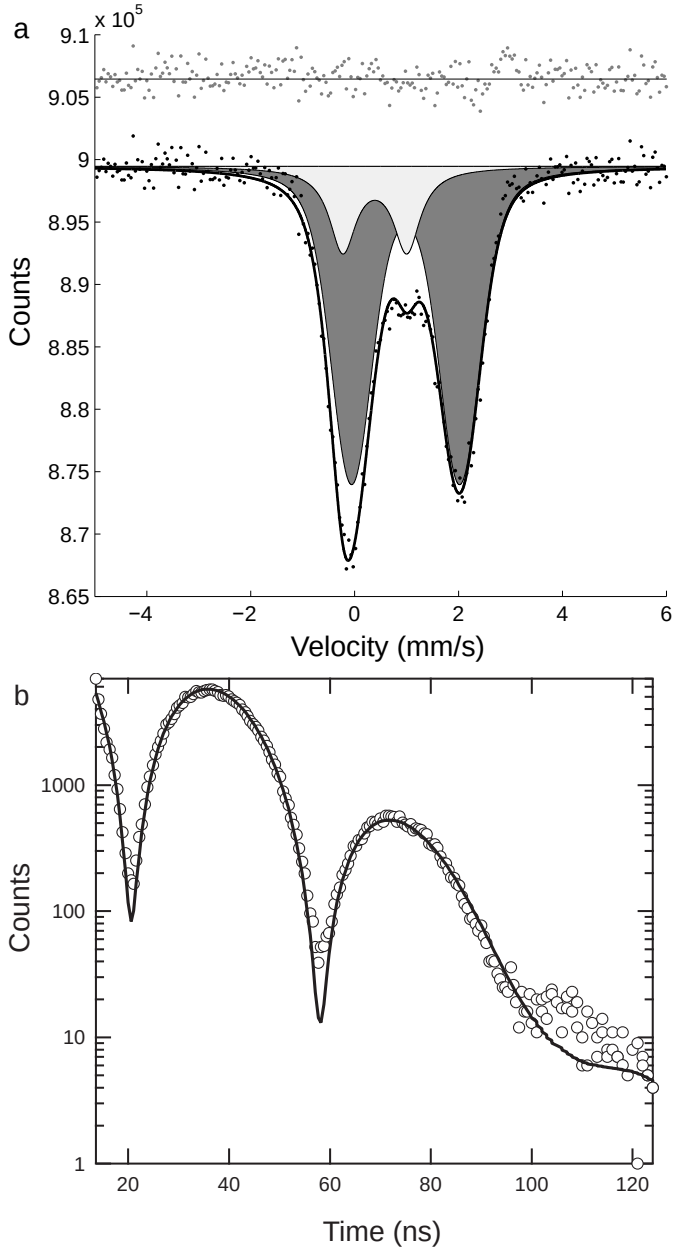


**Figure 1**

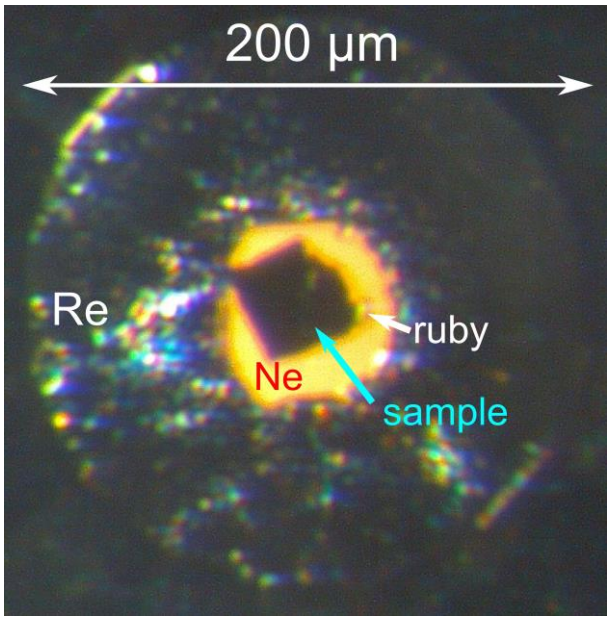


**Figure 2**

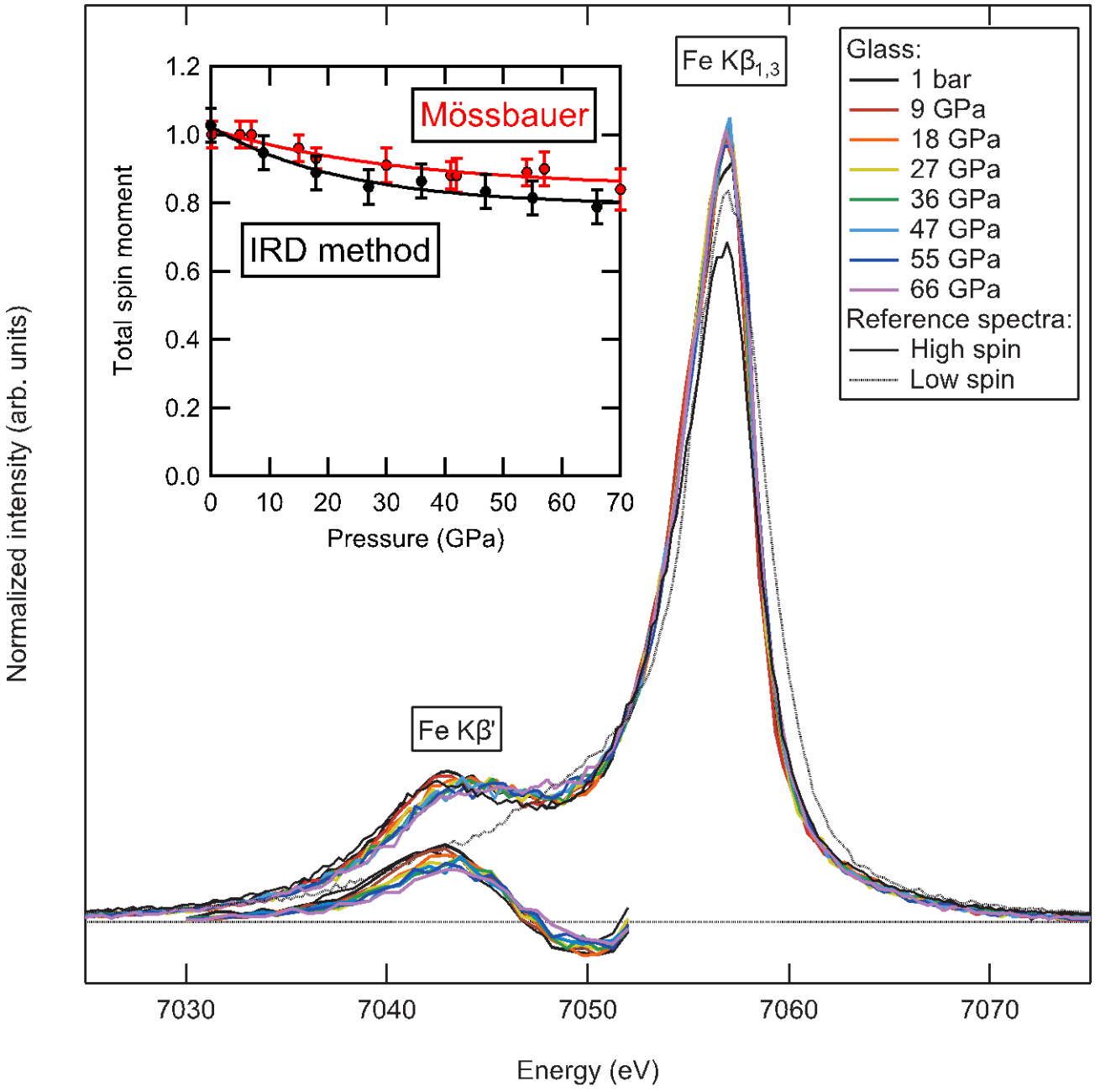


661

662 **Figure 3**

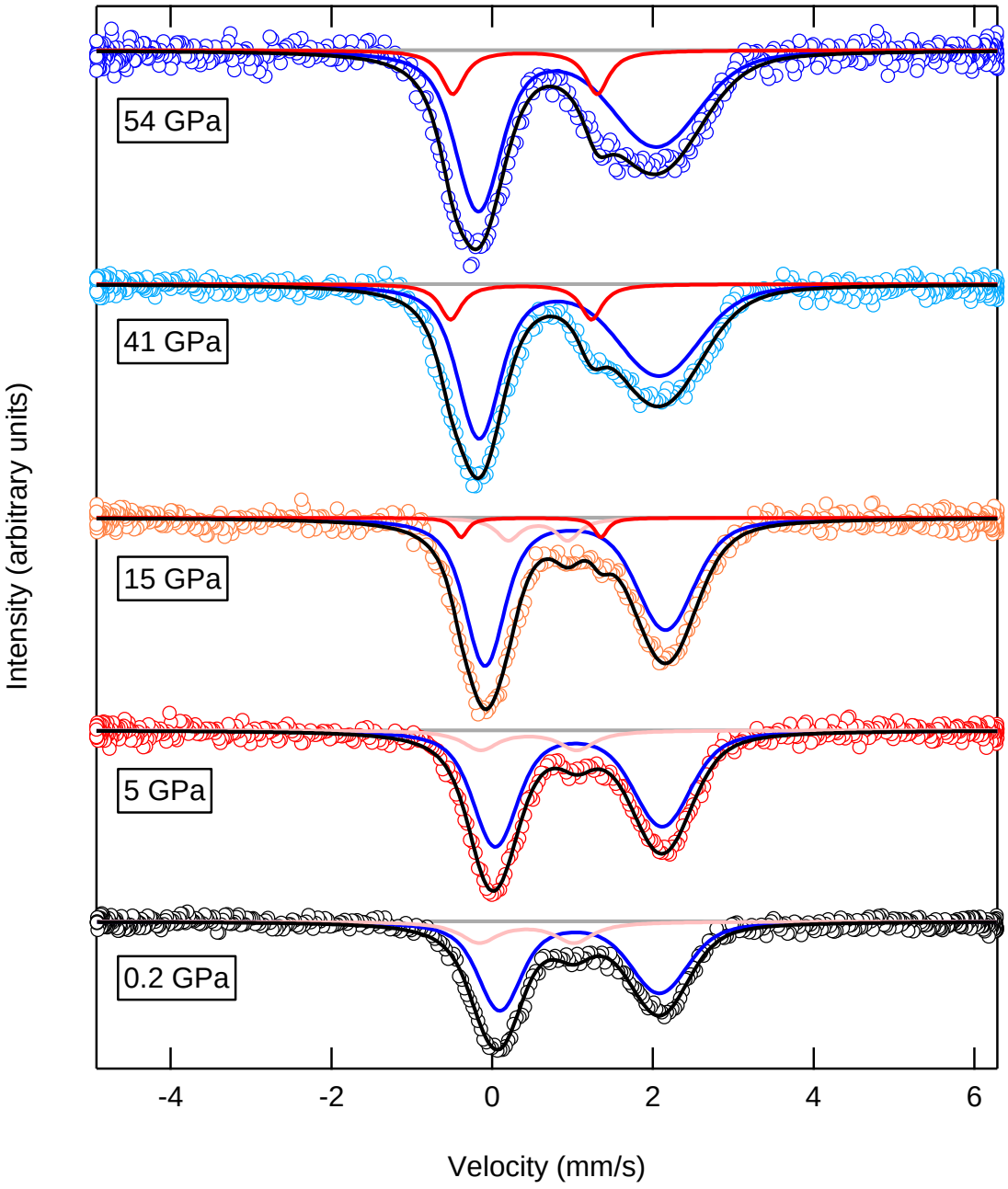


663

664 **Figure 4**

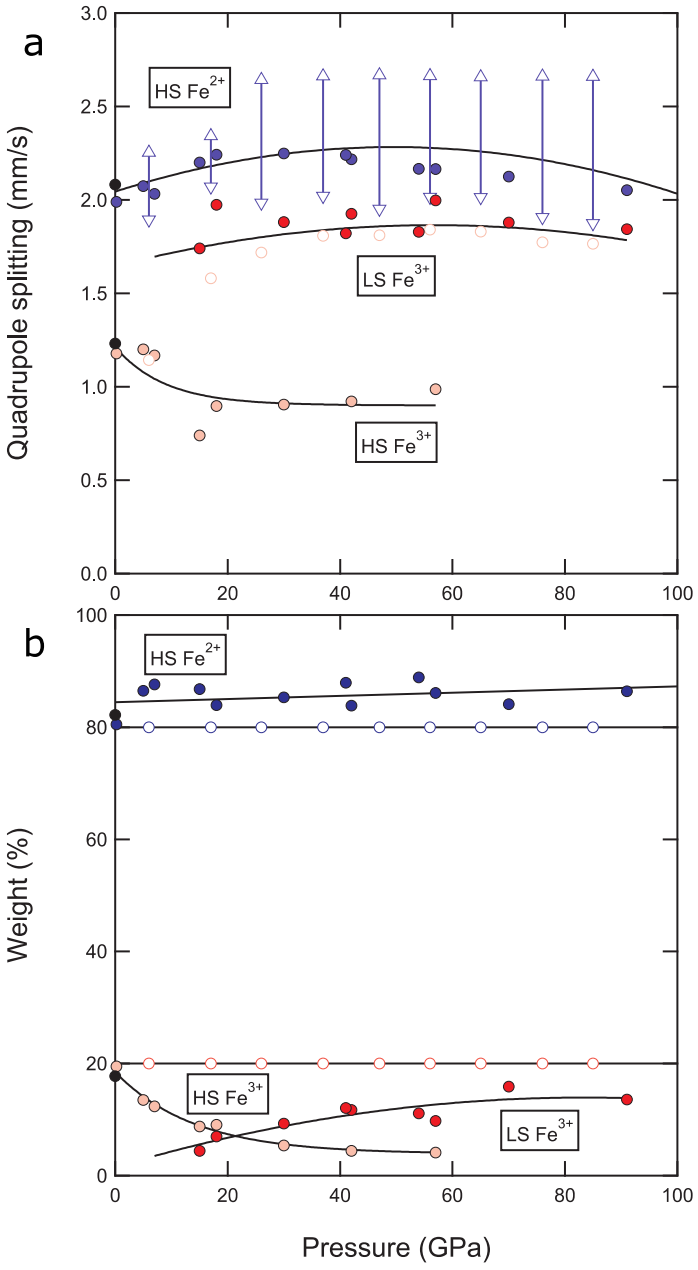


665

666 **Figure 5**

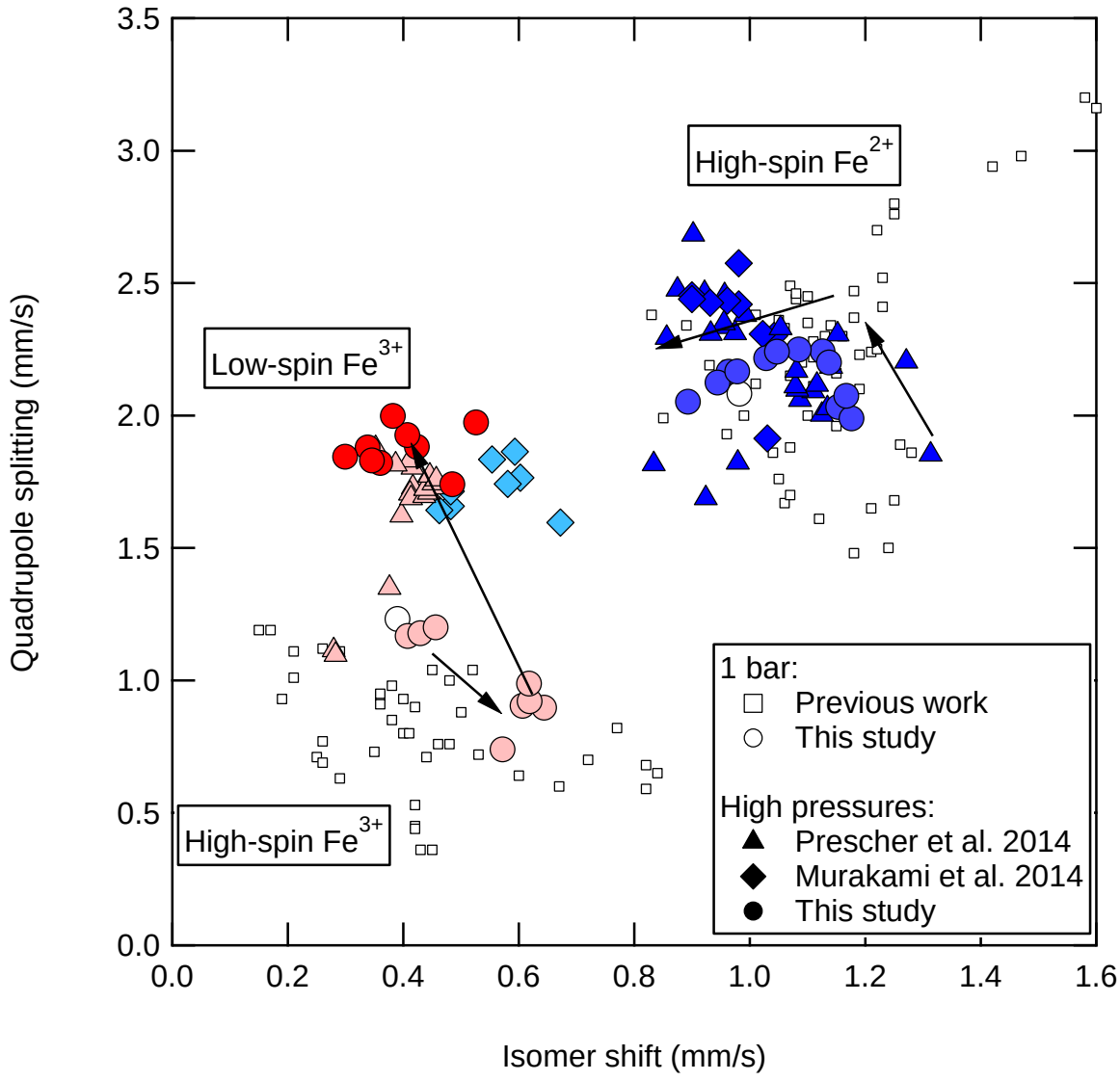


667

668 **Figure 6**

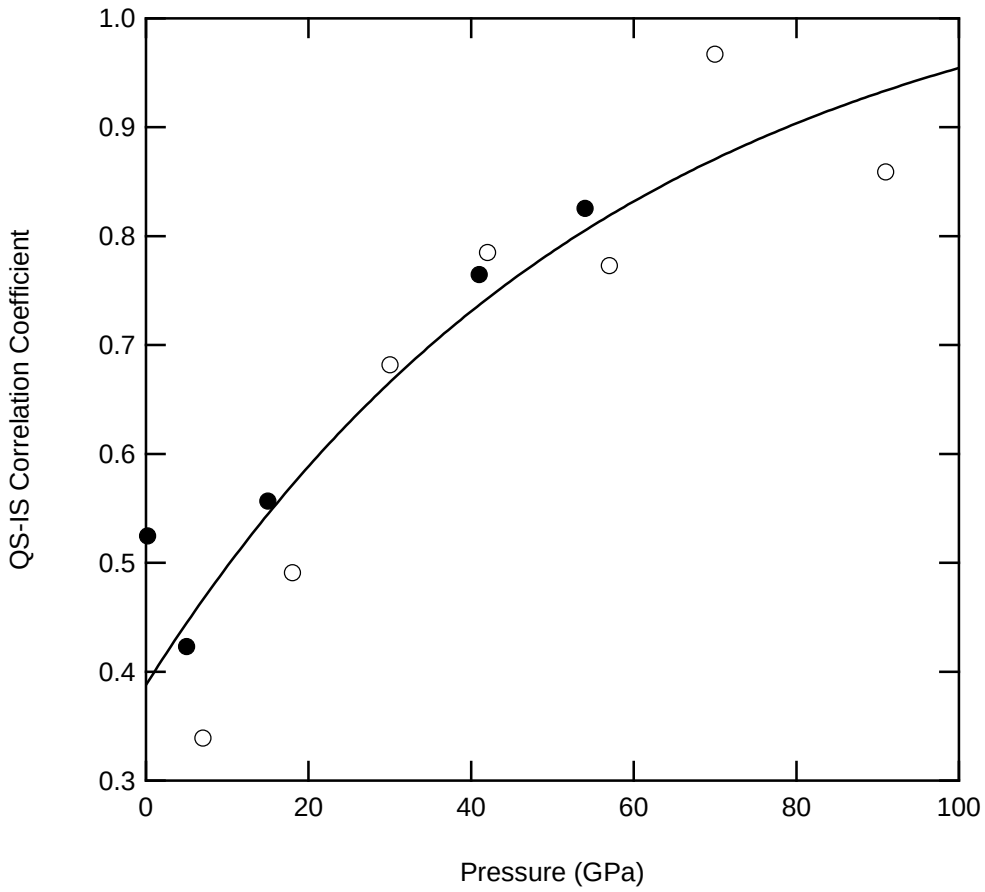


669

670 **Figure 7**